1.8-, 3.3-, and 3.9-μ Bands in Irradiated Silicon: Correlations with the Divacancy*†

L. J. CHENG‡ AND J. C. CORELLI
Department of Nuclear Engineering and Science, Rensselaer Polytechnic Institute, Troy, New York
AND
J. W. CORBETT AND G. D. WATKINS
General Electric Research and Development Center, Schenectady, New York
(Received 28 June 1966)

The annealing behavior and the uniaxial stress response of the radiation-induced defects causing the 1.8-, 3.3-, and 3.9-μ infrared absorption bands were studied after 45-MeV-electron and fast-neutron irradiation. The results indicate that these three bands all arise from the same defect. The defect exhibits two kinds of stress response, as evidenced by the dichroism induced in the bands: one due to electronic redistribution and the other due to atomic redistribution among the allowable orientations. We determine that the defect has an atomic symmetry along a ⟨111⟩ direction and a transition dipole close to a perpendicular ⟨110⟩ direction. The activation energies for atomic reorientation and for annealing of the defect are the same, about 1.2 eV. Correlation of these results with the previous EPR studies indicates that the defect giving rise to these bands is the divacancy. Using the one-electron molecular-orbital model deduced for the divacancy from the EPR studies, some suggestions are given as to the nature of the optical transitions involved.

I. INTRODUCTION

A. General

MANY radiation-induced infrared absorption bands have been observed in silicon. These are at 1.8μ,[1–7] 3.3μ,[3,7] 3.9μ,[3] 5.5μ,[3] 12μ,[7–11] and some bands[7,8,10,11] between 9 and 13 μ.[12] The bands are indicated schematically in Fig. 1.[13] Of these bands, only the 12-μ band has been identified with a specific defect configuration. This band is due to the vibration of the oxygen atom in a vacancy-oxygen complex (i.e., the Si-*A* center[14–16]—recently renamed the Si-*B*1 center[17]). This identification was accomplished primarily by studying the response of the 12-μ band to uniaxial stress and correlating the results with similar experiments done using electron paramagnetic resonance (EPR).

In this paper, we present the results of similar studies on the 1.8-, 3.3-, and 3.9-μ bands produced by 45-MeV electron and by fast-neutron irradiation. From the Fermi level dependence of the 1.8- and 3.3-μ bands, Fan and Ramdas[3] originally suggested that these two bands were due to the same defect. They also observed[8] a stress-induced dichroism which they argued was due to electronic reorientation and that the character of the dichroism was consistent with what they termed a ⟨110⟩ defect symmetry. We find that all three bands show a similar behavior in a variety of different stress experiments, as well as common annealing behavior, etc., arguing they all arise from the same defect. Moreover from correlative information available from previous EPR experiments[18–20] we find that the behavior of these bands correlates closely with the behavior of the divacancy. To facilitate the presentation we will summarize the published divacancy properties and,

* The major part of this research was supported by National Aeronautics and Space Administration under grant NsG-290.
† This paper is taken from the Ph.D. thesis of L. J. Cheng submitted to the faculty of the Physics Department at Rensselaer Polytechnic Institute.
‡ Present address: Metallurgy Research Branch, Atomic Energy of Canada Ltd., Chalk River, Ontario.
[1] M. Becker, H. Y. Fan, and K. Lark-Horovitz, Phys. Rev. **85**, 730 (1952).
[2] H. Y. Fan, Repts. Progr. Phys. **19**, 107 (1956).
[3] H. Y. Fan and A. K. Ramdas, J. Appl. Phys. **30**, 1127 (1959).
[4] V. S. Vavilov, A. F. Plotnikov, and G. V. Zakhvathkin, Fiz. Tverd. Tela **1**, 976 (1959) [English transl.: Soviet Phys.—Solid State, **1**, 894 (1959)].
[5] E. N. Lotkova, V. S. Vavilov, and N. N. Sobolev, Opt. i Spektroskopiya **13**, 216 (1962) [English transl.: Opt. Spectry. (USSR) **13**, 118 (1962)].
[6] E. N. Lotkova, Fiz. Tverd. Tela **6**, 1905 (1964) [English transl.: Soviet Phys.—Solid State **6**, 1500 (1964)].
[7] J. C. Corelli, G. Oehler, J. F. Becker, and K. J. Eisentraut, J. Appl. Phys. **36**, 1787 (1965).
[8] H. Y. Fan and A. K. Ramdas, in *Proceedings of the International Conference on Semiconductors Physics, 1960* (Czechoslovakian Acedemy of Science, Prague, 1961), p. 309.
[9] J. W. Corbett, G. D. Watkins, R. M. Chrenko, and R. S. McDonald, Phys. Rev. **121**, 1015 (1911).
[10] J. W. Corbett, G. D. Watkins, and R. S. McDonald, Phys. Rev. **135**, A1381 (1964).
[11] A. K. Ramdas and M. G. Rao, Phys. Rev. **142**, 451 (1966).
[12] Radiation also makes the silicon lattice infrared active, giving rise to lattice bands in the range 20–35μ. See, for example, R. J. Collins and H. Y. Fan, Phys. Rev. **93**, 674 (1954); M. Balkanski and M. Nusimovici, Phys. Status Solidi **5**, 635 (1964).
[13] We show in addition a band at 8μ, not previously reported, which was observed in the course of this work. The band was observed in a sample originally doped with 2×10^{18} As/cm³ and is believed to be an electronic excitation. Since as yet systematic observations have not been made on this band we will not dwell on it further.
[14] G. D. Watkins, J. W. Corbett, and R. M. Walker, J. Appl. Phys. **30**, 1198 (1959).
[15] G. Bemski, J. Appl. Phys. **30**, 1195 (1959).
[16] G. D. Watkins and J. W. Corbett, Phys. Rev. **121**, 1001 (1961).
[17] G. D. Watkins, in *Radiation Damage in Semiconductors* (Dunod Cie., Paris, 1965), p. 97.
[18] G. D. Watkins and J. W. Corbett, Phys. Rev. **138**, A543 (1965).
[19] J. W. Corbett and G. D. Watkins, Phys. Rev. **138**, A555 (1965).
[20] G. Bemski, B. Szymanski, and K. Wright, J. Phys. Chem. Solids **24**, 1(1963).

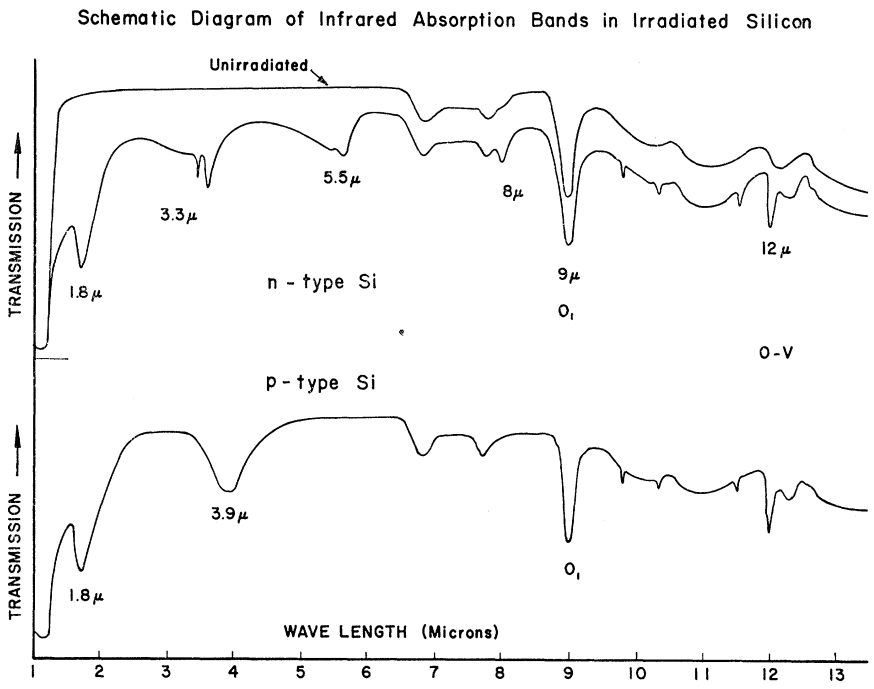

FIG. 1. Schematic diagram of radiation-induced defect infrared absorption bands in silicon (both *n*- and *p*-type) in the wavelength region 1 to 13μ.

after a section describing experimental procedures, use this framework to present the infrared results.

B. Divacancy Properties

The divacancy configuration obtained from the EPR experiments[18–20] is shown in Fig. 2. The adjacent vacancies are designated by the dashed circles, c and c'. The nearest-neighbor atoms to vacancy c' are labeled a, b, and d; those to vacancy c are labeled a', b', and d'. The symmetric divacancy belongs to the D_{3d} symmetry point group. The filling of the orbitals results in a Jahn-Teller distortion and the point-group symmetry is lowered to C_{2h}. More pictorially, we may say that pair-wise bonding of vacancy neighbors occurs.

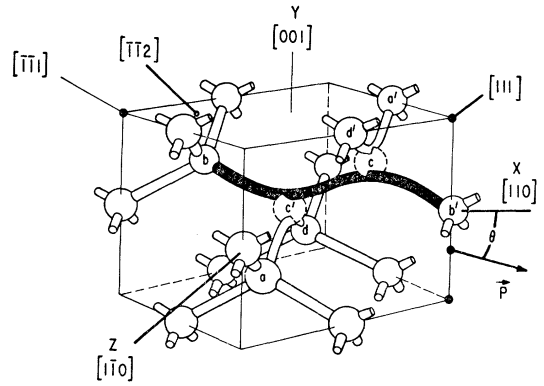

FIG. 2. The model of the divacancy deduced from EPR studies.

The C_{2h} oribtals[21] are shown in Fig. 3. Here as in Ref. 18 we show the one-electron orbitals as made up of linear combinations of the broken bonds (a, b, d, a', b', and d') of the six correspondingly labeled atoms surrounding the divacancy.

The charge state of the divacancy is primarily determined by the filling of b-b' orbitals. The divacancy has net charge (+1) for one electron, and charge (0) for two electrons, in the bonding b-b' orbital; it has charge (−1) for one electron, and (−2) for two elec-

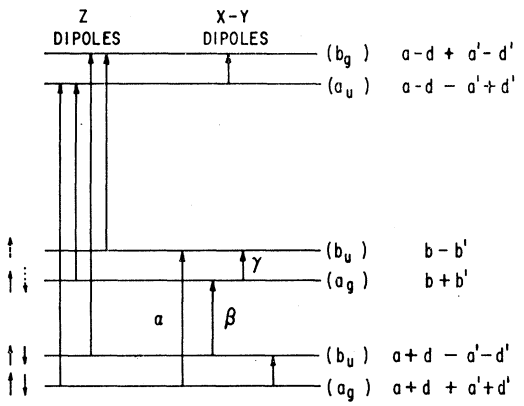

FIG. 3. The one-electron molecular orbital energy levels associated with the divacancy model of Fig. 2. Allowed electric-dipole transitions are indicated.

[21] Admixtures between the a_g and b_u states, respectively, are allowed by symmetry, but these are found to be small in the EPR studies (Ref. 18) and for simplicity, we refer to the orbitals as simply b-b', etc.

trons, in the antibonding b-b' orbital. The states in the forbidden gap corresponding to these charge states are shown in Fig. 4(a). The Fermi level dependence of the infrared (IR) bands that was found by Fan and Ramdas[3] is shown in Fig. 4(b).

There are two types of optical transitions that we might anticipate for the divacancy. First there are electronic transitions to excited localized "molecular" states visualized in Fig. 3 as transitions between the one-molecular orbitals. The allowed transitions can be worked out by straightforward group-theoretical techniques or can be found in papers by Kaplyanskii[22] who has tabulated the allowed electric-dipole and magnetic-dipole selection rules for noncubic defect centers in cubic crystals. The electric-dipole transitions are shown in Fig. 3. As is indicated the transitions either have their axis along the $[1\bar{1}0]$ direction for the defect in Fig. 2—the Z dipoles, or in the $(1\bar{1}0)$ plane—the X-Y dipoles. As is readily evident, for a given stress the dichroism due to Z dipoles and X-Y dipoles will be radically different and easily identifiable. We will find our IR bands have X-Y type dipoles. However, group theory does not specify where these dipoles lie in the X-Y plane and the angle θ the dipole axis makes with the X axis will remain a parameter to be evaluated by comparison to experiment.

In addition to these "molecular" excitations, we can anticipate transitions between the $b\pm b'$ states and the nearest band edges. These, of course, would be accompanied by photo conductivity. For these, group theory allows transitions for all dipole moment directions. However, because of the extended character of the $b\pm b'$ orbitals along the [110] direction, we anticipate here too that the dominant oscillator strength will be in the $[1\bar{1}0]$ plane and with θ close to zero.

The divacancy is found to exhibit two kinds of response to an applied uniaxial stress: electronic and atomic. The electronic response occurs because the electronic configuration shown in Fig. 2 is only one of three possible electronic configurations for the divacancy c-c': namely, the extended orbital can be between atoms b-b' (as shown), atoms a-a', and atoms d-d'. In the unstressed state these three configurations are equivalent energetically. An applied uniaxial stress can lift this degeneracy and, provided sufficient thermal energy is available to overcome the reorientation activation energy, the configurations can re-equilibrate resulting in a net alignment of the defects in the favored configuration. It is found in the EPR studies that this activation energy is only $\sim$0.06 eV and reorientation occurs readily at very low temperatures (i.e., $\gtrsim$20°K). In the atomic response to the applied stress it is the vacancy-vacancy axis that changes, e.g., for the defect shown in Fig. 2, from the [111] to, say, the $[\bar{1}\bar{1}1]$. The barrier for this motion is high enough that equilibration does not take place at room temperature and elevated temperatures are required.

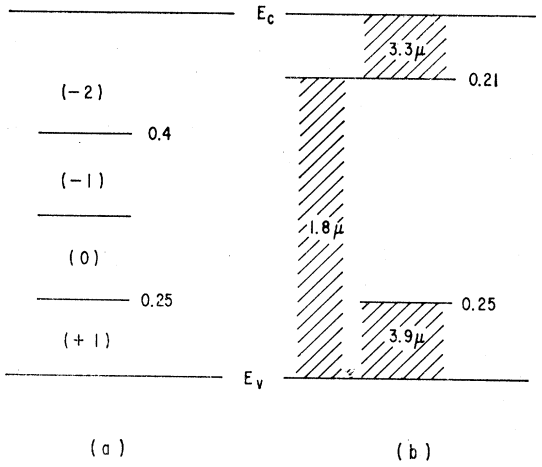

FIG. 4. (a) The energy levels in the forbidden gap corresponding to the different charge states of the divacancy deduced from the EPR studies; (b) the Fermi-level dependence of the IR bands found by Fan and Ramdas. The shaded areas indicate the range in Fermi-level position over which each band is observed.

Because of the anisotropy of the electric-dipole transitions, both types of alignment under stress should produce dichroism[23] in the optical transition allowing a quantitative correlation with the EPR results. In making this correlation, however, a word of caution is in order. Most of the infrared dichroic-ratio studies to be described were performed at room temperature, while the EPR studies were at 20°K. One apparent difference is that at room temperature, the defects can reorient rapidly from one Jahn-Teller direction to another. The effect of this, by itself, can be shown to be unimportant, however, by extrapolation of the reorientation rates determined in the EPR studies. At 300°K, the fastest rate would be $\tau^{-1}\sim 10^{12}$ sec^{-1}. Considering the associated fluctuating direction for the dipole-moment operator, this would contribute a width to the band of $2/(3\pi\tau c)\sim 6$ cm^{-1}. Compared to the observed widths of $\sim$500–1000 cm^{-1}, this is negligible and we can consider the defect as essentially stationary during the optical transition.

However, there is another difference that is not so easily dispensed with. At room temperature, higher vibrational states in the Jahn-Teller wells will be populated and the character of the wavefunction in these states is not necessarily the same as that determined from the EPR at 20°K. It is difficult to estimate the importance of such effects *a priori* and we will have to be guided to some extent by the experimental results. There is certainly reason to be cautious on this point in that at 300°K, kT is approximately one-half the barrier height for reorientation. The amplitudes of vi-

[22] A. A. Kaplyanskii, Opt. i. Spektroskopiya **16**, 602 (1964) [English transl.: Opt. Spectry. (USSR) **16**, 329 (1964)].

[23] By dichroism we mean a difference in the absorption coefficient for light polarized perpendicular and parallel to the stress direction.

bration are therefore sizeable and overlap of the wavefunctions of the different Jahn-Teller distortion states could become important. The result of such effects would probably be to make the dipole-operator direction less well defined, with a corresponding decrease in the magnitude of the observed dichroic ratio.

II. EXPERIMENTAL PROCEDURE

The rectangular bar samples were cut from commerically available silicon ingots [pulled and floating-zone (FZ) crystals]. The orientations of the crystal were determined by means of the growth marks on the ingot.[24] The resistivities of the sample before irradiation were about 100 Ω cm for the n-type crystals and about 0.1Ω cm for the p-type crystals. The surface of the samples through which infrared light was transmitted were polished with diamond compound and 0.3-μ alumina abrasive in order to achieve good transmission.

A Perkin-Elmer Model 21 infrared spectrometer was used to measure the infrared spectra. The spectrometer is constructed in such a way that the sample is put before the monochromator and exposed to the light beam having all wavelengths. For this reason we may observe simultaneously bands characteristic of different charge states of the same defect. A pair of AgCl polarizers were mounted in the spectrometer at a fixed position, and the samples were rotated through 90° in order to measure the dichroic ratio. A glass cryostat was used for measurements taken at liquid-nitrogen temperature. A hydraulic press was used in the *in situ* stressing experiments at room temperature. The same equipment also was used for the stressing experiments at higher temperature by introducing a small oil bath around the sample in the setup. The isochronal- and isothermal-annealing experiments were carried out in a temperature-controlled oil bath for temperatures $\lesssim$275°C and in an oven for higher temperatures.

Most of the samples were irradiated with 45 MeV electrons from the RPI linear accelerator. The samples were immersed in a circulating cold-water bath during irradiation which maintained a sample temperature of $\lesssim$40°C. The rest of the samples were irradiated with fast neutrons obtained from (γ,n) reactions of bremsstrahlung radiation caused by an electron beam incident on a tungsten target.

In order to obtain accurate information concerning the dichroism in the 1.8-, 3.3-, and 3.9-μ bands we need to know the background absorption at these bands. Since we observed no band shift or splitting in these bands under stress, the dichroism itself provides a tool for evaluating the background. The absorption corresponding to the different polarizations arises from different numbers of defects absorbing in that orientation while the background appears to remain constant. To evaluate the background we require that the band

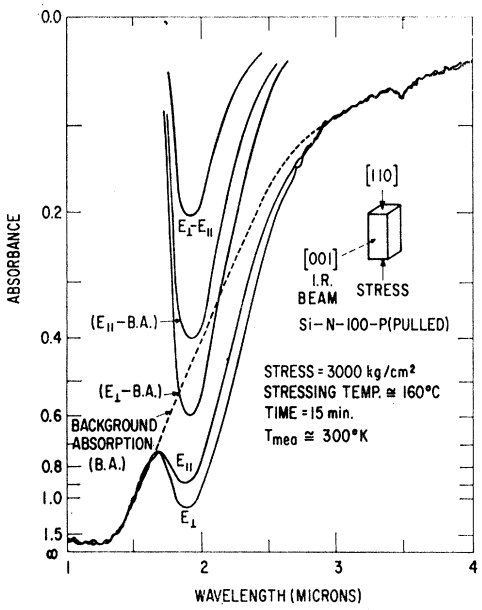

FIG. 5. The quenched-in dichroism exhibited by the 1.8-μ band at room temperature as a result of 15-min stress at ~160°C.

shape for each polarization be the same and further that the background so obtained be smooth, i.e., contain no vestige of the band. Examples of this analysis for each of the bands are shown in Figs. 5, 6, and 7. The background at the 1.8-μ band is particularly troublesome because this background is in itself due to a radiation

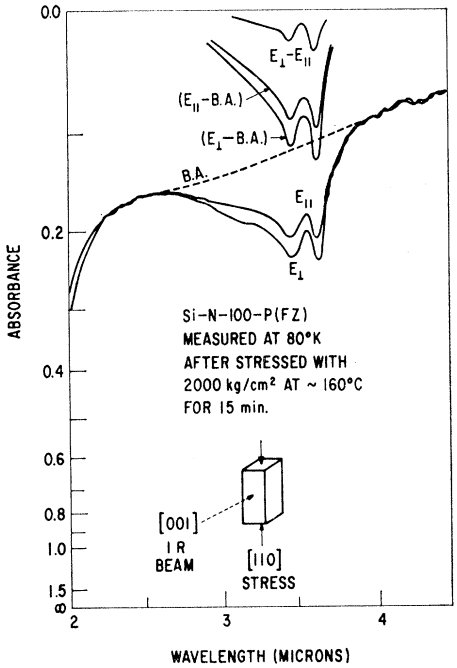

FIG. 6. The quenched-in dichroism exhibited by the 3.3-μ band at 80°K resulting from 15-min stress at ~160°C.

[24] R. D. Hancock and S. Edelman, Rev. Sci. Instr. 27, 1082 (1956).

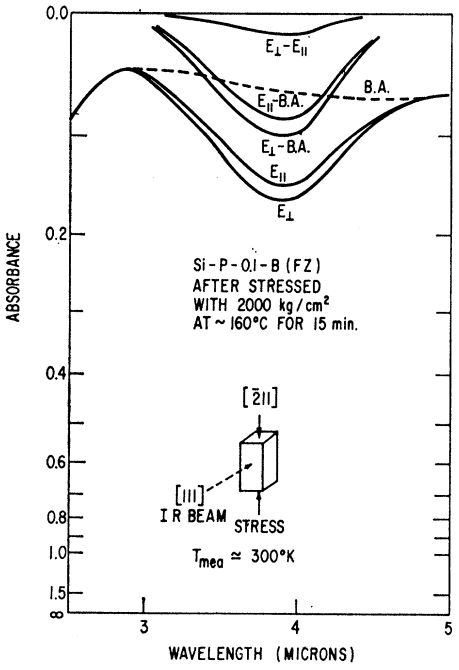

FIG. 7. The quenched-in dichroism exhibited by the 3.9-μ band at room temperature resulting from 15-min stress at ~160°C.

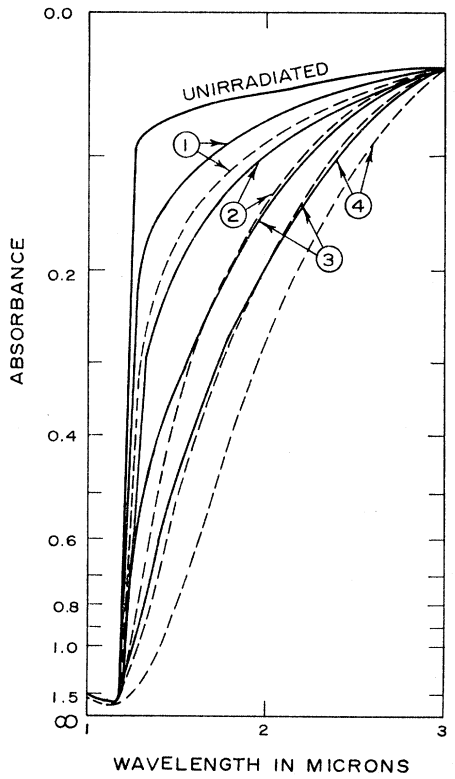

FIG. 8. The radiation-induced near-edge absorption band in pulled and floating-zone n-type samples after various doses of 45-MeV electron irradiation. (The curves have been normalized at 3μ.) —FZ samples; - - - pulled samples; ① 1.8×10^{18} e/cm²; ② 2.0×10^{18} e/cm²; ③ 3.0×10^{18} e/cm²; ④ 6.5×10^{18} e/cm².

produced band, which was termed by Fan and Ramdas[3] "the absorption edge band." They suggested it arose due to a modification of the band edges due to the introduction of defects. Using the procedure above we were able to separate the 1.8-μ band from this near-edge absorption band. These results are shown in Fig. 8. We will do nothing further with these results in this paper than to note that the production rate of this band is somewhat higher in the pulled samples than in the floating-zone samples.

III. RESULTS AND COMPARISON TO THE EPR DIVACANCY STUDIES

As indicated in the Introduction we find that the stress-response behavior of the 1.8-, 3.3-, and 3.9-μ bands correlates with the EPR divacancy measurements and therefore we will present our results *vis a vis* the EPR results.

A. Room-Temperature Stress Studies

The application of uniaxial stress *in situ* at room temperature produces sizeable dichroism in the 1.8- and 3.9-μ bands. The results of a quantitative study for various stress and viewing directions is given in Table I. We also indicate the 1.8-μ data of Fan and Ramdas[8] determined at 300 and 77°K, and the 3.3-μ data of Rao

TABLE I. Dichroic ratios of the 1.8-, 3.3- and 3.9-μ bands under stress at room temperature.

Stress direction	Magnitude of stress (kg/cm²)	IR beam direction	$\alpha(E_\perp)/\alpha(E_\parallel)$ Experimental 1.8μ	3.3μ	3.9μ	Calculated $\theta=-5°$	$-10°$	$-15°$
[100]	1900	[1$\bar{1}$0]	0.78,(<1)[a]	(<1)[b]		0.71	0.73	0.76
[100]	1450	[1$\bar{1}$0]		(<1)[b]	0.74	0.76	0.78	0.80
[110]	2000	[001]	1.25	(>1)[b]		1.46	1.37	1.29
[110]	1500	[001]		(>1)[b]	1.33	1.33	1.28	1.22
[110]	...	...	(>1)[a]	(>1)[b]				
[111]	2000	[1$\bar{1}$0]	1.28	...		1.36	1.29	1.22

[a] Rao and Ramdas (Ref. 25), observed at 77°K.
[b] Fan and Ramdas (Ref. 8), observed at 300°K and 77°K.

TABLE II. Dichroic ratios of the 1.8-, 3.3-, and 3.9-μ bands after stressing at 160°C for 15 min.

Stress direction	Magnitude of stress (kg/cm²)	IR beam direction	$\alpha(E_\perp)/\alpha(E_\parallel)$ Experimental 1.8μ	3.3μ	3.9μ	Calculated $\theta=-5°$	$-10°$	$-15°$
[110]	2000	[001]	1.29	1.24		1.29	1.35	1.40
[110]	3000	[001]	1.44	1.46		1.51	1.62	1.73
[110]	3000	[1$\bar{1}$0]	1.27	1.24		1.27	1.32	1.47
[110]	1580	[001]	1.26		1.25	1.21	1.25	1.29
[111]	2100	[1$\bar{1}$0]	1.33			1.20	1.24	1.28
[$\bar{1}\bar{1}$2]	2000	[111]	1.26		1.22	1.15	1.19	1.22
[001]	2100	[1$\bar{1}$0]	1.0	1.0		1.00	1.00	1.00
[001]	1500	[$\bar{1}$10]	1.0		1.04	1.00	1.00	1.00

and Ramdas[25] determined at 77°K. Both of these latter were terse conference reports and did not provide sufficient information for us to arrive at quantitative values for the dichroism. Qualitatively, however, these data can be seen to agree with our data and serve the additional purpose of demonstrating that similar dichroism is introduced into the 3.3-μ band.[26] For their low-temperature stress studies, a differential thermal expansion was used to apply the stress[25] and neither the temperature at which the stress is applied nor its magnitude was well defined. However, the large effects observed by these authors allowed them to conclude that reorientation could take place at well below room temperature, consistent with an electronic reorientation.

We will defer a quantitative comparison of the data of Table I with the divacancy until Sec. IV. We only note here that the presence of this stress-induced dichroism for all bands at or below room temperature is consistent with expectations for the "electronic" reorientation between the equivalent Jahn-Teller distortions of the divacancy.

B. Elevated-Temperature Stress Experiments

Table II shows the dichroism obtained on the 1.8,-3.3-, and 3.9-μ bands by stressing for 15 min at 160°C and cooling the samples to room temperature with the stress on. The stress was then removed for measurement on the frozen-in dichroism. Typical results are shown in Figs. 5, 6, and 7. Again, we will defer the quantitative comparison of the Table II results with the EPR data until Sec. IV.

We have also studied the loss of this dichroism upon

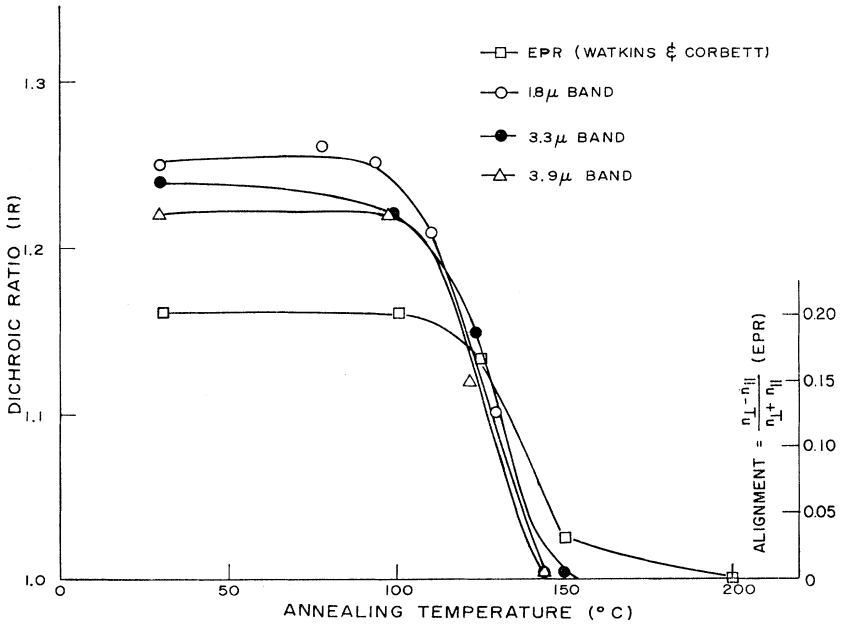

FIG. 9. Isochronal (15-min) anneal of the quenched-in dichroism in ⟨110⟩-stressed crystals for the three IR bands. Also shown is the anneal of the quenched-in divacancy alignment as studied by EPR (Fig. 11 of Ref. 18).

[25] M. G. Rao and A. K. Ramdas, Bull. Am. Phys. Soc. **10**, 123 (1965).

[26] In our samples the 3.3-μ band could be observed only at low temperature and could therefore not be studied in the room-temperature squeezing apparatus used in our experiment.

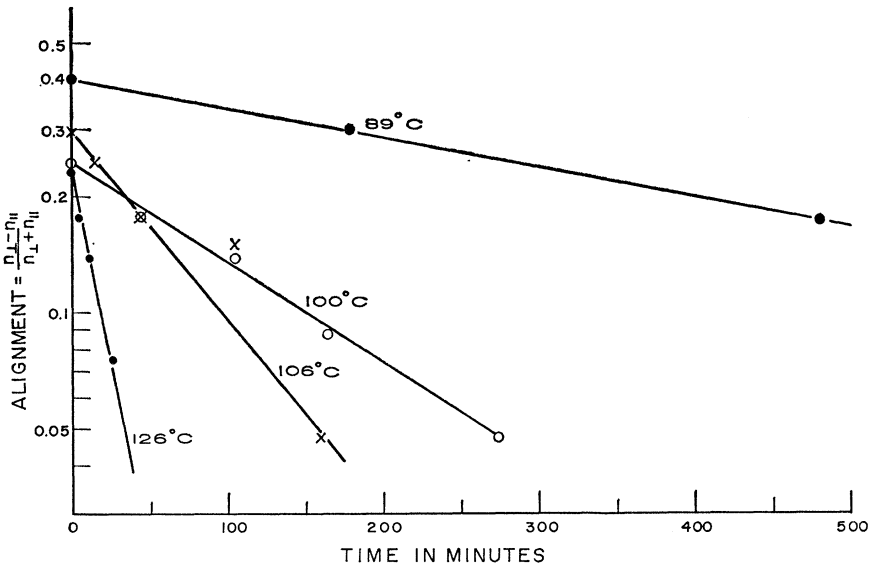

FIG. 10. Isothermal anneals of the quenched-in alignment as determined from the dichroism of the 1.8-μ band in ⟨110⟩-stressed crystals. In the ordinate, $n_\perp$ is the number of divacancies with their axes perpendicular to the stress direction and $n_\parallel$ is the number in the other orientation. These numbers were determined from the observed dichroic ratios using the formulas in the Appendix with $\theta = -5°$.

annealing in the unstressed state. Isochronal-annealing results are shown in Fig. 9 together with the loss of the divacancy alignment as determined by EPR. It can be seen that the loss of defect alignment for all three bands correlates closely with that for the divacancy. In Fig. 10 we show similar results for isothermal experiments. The half-lives for recovery of these isothermal experiments together with a lower temperature experiment are shown in Fig. 11. The slope of the line through these points gives an activation energy of 1.25 eV. (The EPR measurements in loss of alignment were isochronal only but by assuming a frequency factor of 10^{13} sec^{-1}, they were analyzed as indicating an activation energy of $\sim$1.3 eV, fully consistent with our measured $E=1.25$ eV.) Since the mean number of jumps per defect for the loss of the dichroism is 1, we may obtain the frequency factor for this process $-\sim 8\times 10^{12}$ sec^{-1}.

The existence of the quenched-in dichroism plus the close correlation of the reorientation kinetics, constitutes additional confirmation of the identification of these bands with the divacancy. One additional important confirmation is evident from Table II. All three bands give no evidence of dichroism for a ⟨100⟩ stress confirming the ⟨111⟩ atomic axis for the defect. (All four ⟨111⟩ directions make the same angle with respect to the ⟨100⟩ axis and are therefore equivalent.)

C. Damage Recovery

In Figs. 12 and 13 are shown the disappearance of the 1.8- and 3.3-μ bands upon annealing. It will be noticed that in the FZ samples some loss of the bands occurs at $\sim$160°C. From the data in Fig. 11 we see that the defects could make $\sim$10 jumps in this stage. Since it seems unlikely that this number of jumps could give the significant loss of defects, we attribute this stage rather to the onset of migration of other defects and they in turn either annihilate or sufficiently alter the defects giving rise to the IR bands so that they no longer contribute to the absorptions. We have made isothermal measurements on the remaining high-temperature recovery stage for the 1.8-μ band in floating-zone silicon. These are shown in Fig. 14. The half-time for recovery of these data is shown in Fig. 11, as is similar data in pulled silicon obtained by Fan and Ramdas.[3] (They had analyzed their data as indicating an activation energy of 0.8 eV but now concur that it should be $\sim$1.2 eV.) All three lines in Fig. 11 indicate an activation energy 1.2 eV. Since the loss of atomic alignment requires the motion of the divacancy in the lattice we see that these energies should be the same for the divacancy. The faster anneal in pulled silicon is consistent with the identification of oxygen as an effective

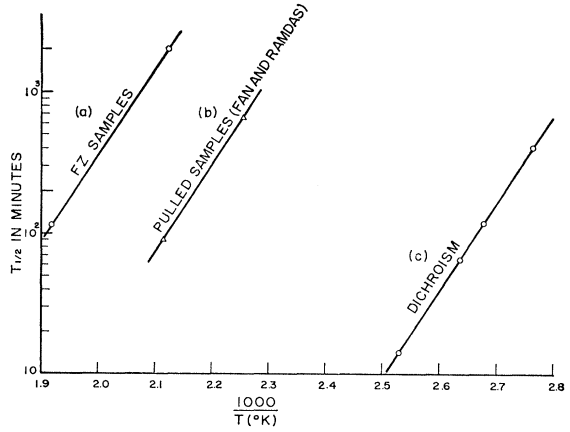

FIG. 11. Time of 50% anneal versus $1000/T$ for (a) anneal of the 1.8-μ band in floating-zone silicon, (b) anneal of the 1.8-μ band according to Fan and Ramdas, and (c) anneal of the dichroism of the 1.8-μ band.

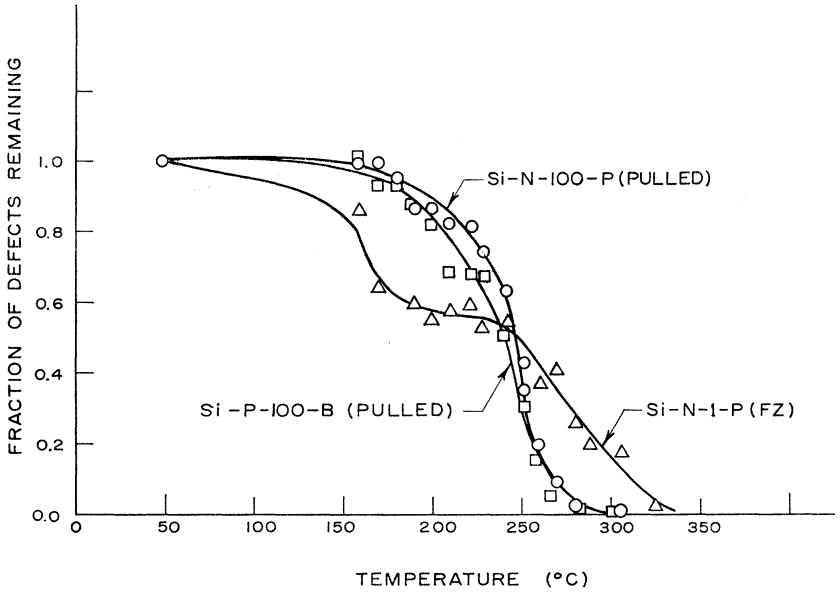

FIG. 12. Isochronal anneal (20 min at each temperature) of the 1.8-μ band in pulled and in floating-zone silicon.

trap for the mobile divacancies. We have additional experimental evidence for the oxygen as a trap for divacancies in that the Si $B1$ centers (12-μ band) increase in number as the divacancy anneals out.

Direct comparison of the data of Figs. 12 and 13 with the EPR annealing results is made difficult because different temperature intervals (10° vs 50° for the EPR) and annealing times (20 min vs 15 min for the EPR) were used. However, using $E=1.25$ eV, we may convert the annealing curves of Figs. 12 and 13, to the equivalent curves for the isochronal annealing sequence used in the EPR. The results determined from two of the curves of Fig. 13 are shown in Fig. 15. Again we see the close correlation of the data both from the general region where annealing is occurring and in the constant difference between floating-zone and pulled silicon.

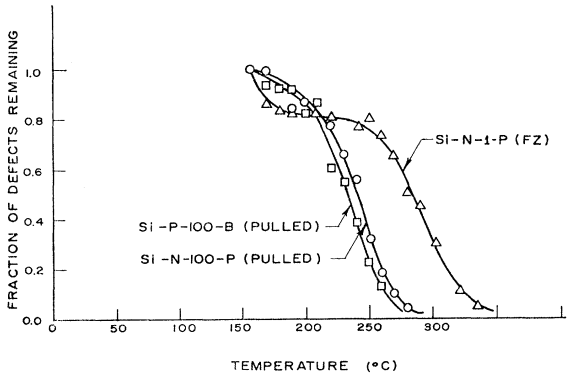

FIG. 13. Isochronal anneal (20 min at each temperature) of the 3.3-μ absorption band in pulled and in floating-zone silicon.

IV. DISCUSSION

A. Dichroic Ratios

The energy of a defect in a stress field can be expressed in a multipole expansion. The lowest order term is due to what Nowick and Heller[27] call an "elastic dipole." The energy of an elastic dipole is related to the strain tensor, a second-rank tensor, by a second-rank tensor:

$$E=\sum_{ij} B_{ij}\epsilon_{ij}. \quad (1)$$

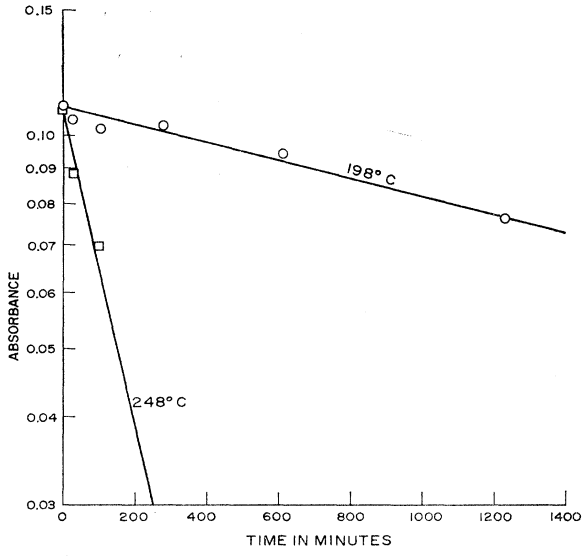

FIG. 14. Isothermal anneal of the 1.8-μ band at 198°C and 248°C.

[27] A. S. Nowick and W. R. Heller, Advan. Phys. **12**, 251 (1963).

Kaplyanskii[22] has shown that for the symmetry characterizing the divacancy, which in his notation is a type-I monoclinic center, the matrix **B** has only four independent parameters.

In the X, Y, Z axis a system shown in Fig. 2, symmetry considerations show that for the divacancy the **B** matrix has the form

$$\mathbf{B}=\begin{bmatrix} B_1 & B_4 & 0 \\ B_4 & B_2 & 0 \\ 0 & 0 & B_3 \end{bmatrix}. \tag{2}$$

In experiments such as ours which are insensitive to the *hydrostatic* component of strain, (i.e., the trace of **B**), the number of independent parameters are further reduced to three.

The EPR divacancy measurements[18] for both electronic and atomic reorientation were performed for for only a ⟨110⟩ uniaxial stress. In those experiments, it was found that one parameter sufficed to describe the stress response in both types of reorientation. In terms of **B**, the analysis assumed $B_1=B_2=B_4=0$ and $B_3=M$. Viewed more physically this parameter M was described as the energy change per unit strain along the "bonding" atom direction—the a-d, a'-d', or Z axis in Fig. 2:

$$M=(dE/d\epsilon)_{\mathrm{Si-Si}}. \tag{3}$$

In the electronic reorientation in the EPR, M was found to be $\sim+24$ eV/unit strain for the $(+1)$ charge state of the divacancy and $M\sim+32$ eV/unit strain for the (-1) charge state. For the atomic reorientation, an average value, $M\sim28$ eV/unit strain, was found adequate to describe the stress response. Assuming that this M (or B_3) dominates the stress response and assuming a well-defined dipole moment for the transition at an angle θ in the XY plane (see Figs. 2 and 3), we can calculate explicit formulas for the dichroic ratios shown in Tables I and II. These calculations are outlined in the Appendix and the results[28] are shown in Figs. 16 and 17. In these figures, the horizontal bars indicate the values of the observed dichroic ratios from Tables I and II.

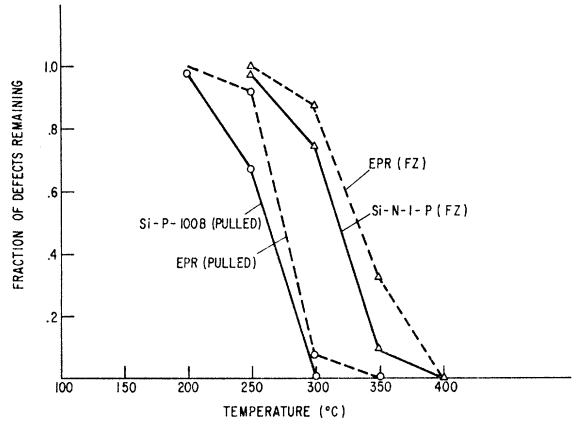

FIG. 15. Comparison of the anneal of the 3.3-μ band (Fig. 13) with the divacancy anneal as studied by EPR. The IR results have been converted to the equivalent isochronal sequence used in the EPR studies (50° interval, 15-min duration), by using an activation energy of 1.25 eV.

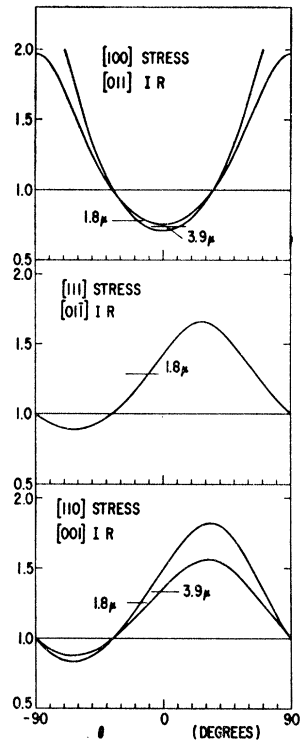

FIG. 16. Calculated and observed dichroic ratios for the room-temperature electronic redistribution of the divacancy under uniaxial stress for the various experimental conditions described in Table I.

Because of the different dependence upon θ of the electronic and atomic dichroism, we see that the allowed value for θ for all bands is restricted to a narrow range around 0°. For comparison to the experimental results, the value predicted for several values of θ are included in Tables I and II. For the 3.3- and 3.9-μ bands we see that the choice $\theta=-5°$ gives remarkable agreement for all stress experiments in both tables. The 1.8-μ band fit in Table II and $\theta=-5°$ is good but the fit in Table I is better with $\theta=-15°$. A choice of $\theta=-10°$ for the 1.8-μ band is probably the best compromise with a resulting uniform tendency for somewhat smaller dichroism than predicted.

We feel that this close agreement constitutes strong confirmation of the identification of these bands with the divacancy. In all cases the sense and relative magnitude of the predicted dichroism is borne out. We believe the small uniform reduction in the observed dichroism for the 1.8-μ band though real, does not represent a serious inconsistency with the model. This probably reflects the reservations expressed in Sec. II,

[28] For these, the average value $M=28$ eV/unit strain previously estimated from the EPR results was used, and a correction for the estimated 95% polarizer efficiency has been included. We have used 150°C as the effective temperature in the high-temperature experiments.

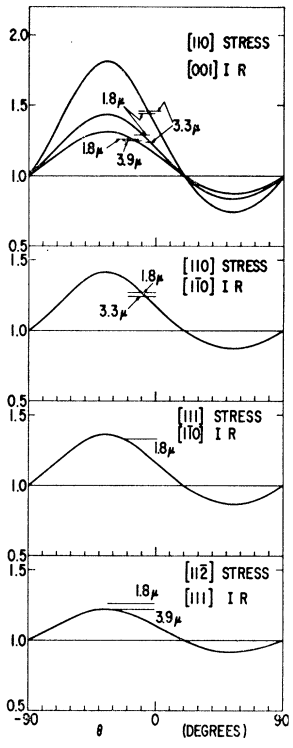

FIG. 17. Calculated and observed dichroic ratios due to the quenched-in atomic alignment of the divacancy after 150°C stressing for the various experimental conditions described in Table II.

that the transition dipole axis is not so well defined for this transition. We will return to this point in the next section. Indeed, the over-all agreement is quite remarkable considering the over-simplified model for the calculation, i.e., the ignoring of other components of the B tensor of Eq. (2).

Similar calculations for the dipole-moment axis assumed along the Z-direction of Fig. 2 immediately rules out this possibility. In particular, most of the predicted dichroic ratios of Tables I and II are reversed in sense from that observed. The determination of the transition-dipole-moment is thus unique.

B. Other Features

There are several other general observations that are consistent with the identification of these bands with the divacancy. First, we can conclude that the intensity of the bands is not inconsistent with the number of divacancies that should be present. We estimate the number of divacancies from the production rate of 0.035 cm^{-1} for 45-MeV electrons determined by EPR.[19]. From the integrated intensity of the 1.8-μ absorption band, we conclude that the necessary oscillator strength[29] is only $\sim$0.05. Second, as has been noted by several authors,[3,7,8] the 1.8-μ band does not appear to correlate with any known impurity, consistent with the identification with an intrinsic defect.

If has been noted by Fan and Ramdas[3] that the presence of oxygen greatly enhances the production rate of the 1.8-μ band for 4.5-MeV electron irradiation but not for neutron irradiation. In our experiments at 45 MeV, we note also a production rate approximately 50% greater for the IR bands in pulled samples over floating-zone samples. On the other hand, in previous EPR studies at $\sim$1 MeV, the production rates for divacancies did not show any large variation between these materials. This apparent lack of correlation may reflect the much larger dose used in the IR work. In any event this role of oxygen is not understood and the production process needs further study.

C. Nature of Optical Transitions

In Fig. 4 we show that electrical level structure inferred from EPR for the divacancy along with the Fermi level requirements for the observation of the bands, as reported by Fan and Ramdas.[3] Here we include our observation that the 1.8-μ band is observed in low-resistivity p-type materials as well, a question left unanswered by Fan and Ramdas.

Fan and Ramdas reported no photoconductivity associated with the 1.8-μ band. This strongly suggests that this transition is to some kind of localized molecular excitation, and that the excited state is in poor "contact" with the conduction or valence bands. We therefore look to the one-electron molecular states of Fig. 3 as a guide to the kind of excitation involved.

From Fig. 4 we see that the 1.8-μ band is present for several charge states of the divacancy but disappears when the Fermi level rises above $\sim E_c-0.21$ eV. This suggests that the disappearance is associated with the change from the single-minus to double minus-charge stage of the divacancy, estimated from EPR studies to occur at $\sim E_c-0.4$ eV. The discrepancy in these values for the energy could be the result of errors in either or both measurements. Both estimates were made by rough monitoring of the Fermi level versus emergence of the relevant EPR or IR spectrum. Since both experiments were performed under conditions where the divacancy was probably not the dominant defect, and under conditions where considerable inhomogeneity in Fermi level position may have been present, error could be present in both measurements. Levels near both $E_c-0.21$ eV and $E_c-0.4$ eV have been detected in electrical measurements.[30] Further study is clearly necessary in order to be conclusive on this point. We will assume here, however, that the uncertainties in both measurements adequately accommodate the identification as the same level.

From Fig. 3, we see that the change from the single-minus to double-minus charged state corresponds to the filling of the b-b' orbital. Both transitions α and γ vanish upon the filling of the orbital, while they continue to

[29] See D. L. Dexter, in *Solid State Physics*, edited by F. Seitz and D. Turnbull (Academic Press Inc., New York, 1958), Vol. 6, p. 359. In this estimate we have taken $\epsilon_0/\epsilon_{eff}=1$.

[30] See, for example, E. Sonder and L. C. Templeton, J. Appl. Phys. 34, 3295 (1963).

exist for the other charge states in agreement with the experimental observations. Both transitions have their dipole moments in the X-Y plane and because of the extended nature of the b-b' orbital should have $\theta \sim 0°$. The 1.8-μ band corresponds to 0.69 eV which seems large for the γ transition, being between two states which differ mainly by virtue of the weak overlap between the b and b' orbitals. Also it seems hard to understand why this energy difference does not change noticeably with charge state, i.e., as one, two, and three electrons are accommodated by them.

For this reason, we tentatively identify the 1.8-μ band with transition α. This identification further supplies a natural explanation for the breadth of the absorption band. In the transition, an electron is removed from the strongly bonding (Jahn-Teller) states between atoms a, d and a', d' and is transferred to the "nonbonding" b-b' state. The excited state, having only three electrons in the "bonding" orbitals, will have a different (smaller) equilibrium Jahn-Teller distortion. In such systems where the ground- and excited-state equilibrium "configurational" coordinates are different, "vertical" transitions in the Franck-Condon sense can give broad lines because transitions involving many different changes in vibrational quantum number become important. Indeed transitions to high vibrational states of other Jahn-Teller distortion directions may also become important, making the dipole operator direction become less well defined. This plus the fact that at room temperature as mentioned before kT is becoming comparable to the barrier height in the ground state could account for the uniform decrease in the dichroism observed for the 1.8-μ band.

The 3.9-μ band appears only when the Fermi level is above $E_v+0.25$ eV and we therefore identify this transition as arising from the singly positively charged divacancy. Fan and Ramdas[3] measured photoconductivity associated with this band, which suggests that the transition is an excitation of an electron from the valence band edge to the $b+b'$ orbital of Fig. 3. The hole produced in the valence band thus contributes the photoconductivity. In this sample view, the dipole-moment direction reflects primarily the extended character of the $b+b'$ orbital.

The fact that the 3.9-μ band is a well-defined band, with oscillator strength comparable to the 1.8-μ band, suggests also looking for an excited localized molecular state in Fig. 3 that is well coupled to the valence band. (The band and localized molecular orbital pictures are not entirely unrelated, of course. The molecular orbitals can be viewed as made up of suitable wave packets from the band states.) Transition β has the required properties, being an XY dipole and existing only for the singly positively charged state.

(We should point out that the relative ordering shown in Fig. 3 for the a_g and b_u states for both the bb' orbitals and for the ad-$a'd'$ orbitals is somewhat uncertain. They were ordered as shown to favor the wavefunction with the least number of nodes, a usually reliable practice in isolated molecules. However in our case, interaction with the conducting and valence bands could well reverse the ordering. For instance, the b_u orbitals might be expected to have strongest interaction with the conduction band and be repelled downward and the a_g states with the valence band, being repelled upward. If the level ordering were reversed, the β transition would be identified with the 1.8-μ band and the α transition the 3.9. This has some appeal in that the remaining hole after the 1.8-μ band excitation would be in the b_u orbital, with poorer contact to the valence band and no photoconductivity. The remaining hole after 3.9-μ excitation would be in the a_g orbital with stronger contact to the valence band with subsequent photoconductivity. Since all of the discussion in this section is speculative in nature, however, we will not elaborate on these finer details further. Indeed, the α and β transitions may be very close in energy, both contributing within the breadth of the 1.8-μ band, and not be involved at all for the 3.9-μ band.)

The 3.3-μ band must arise from the doubly negatively charged state. Since no photoconductivity has been identified with it, it must also be viewed as a transition to a localized "molecular" state. The sharpness of the band and its structure would appear to indicate that large lattice relaxation in the excited state does not take place as it does in the 1.8-μ band, possibly ruling out transitions to and from the bonding or antibonding ad-$a'd'$ states.

There are no XY dipole transitions remaining for the double minus charged state in Fig. 3. There are, of course, other excited molecular states not included in the figure involving excited atomic states ($3d$, $4s$, $4p$, etc.). The 3.3-μ band could be associated with transitions from the b-b' orbital to these.

V. SUMMARY AND CONCLUSIONS

We have presented arguments that the 3.3-, 1.8-, and 3.9-μ bands observed in irradiated silicon all arise from the divacancy. These arguments were based upon several correlations between the behavior of the e bands and the divacancy as previously studied by EPR. Briefly summarized, these arguments were:

1. All three IR bands exhibit stress-induced dichroism at room temperatures which agrees in sense and symmetry and satisfactorily in magnitude with that predicted from EPR studies for the "electronic" reorientation of the divacancy associated with its intrinsic Jahn-Teller distortion.

2. The bands also exhibit additional dichroism quenched-in as a result of stress at $\gtrsim 150$°C, which correlates in sense and symmetry and satisfactorily in magnitude with that associated with the "atomic" reorientation of the vacancy-vacancy axis. The kinetics of this alignment agrees closely with that observed for the divacancy in EPR studies.

3. Annealing studies of the disappearance of the bands correlate with that observed in EPR. This correlation also shows up in consistent differences between the annealing behavior in pulled and floating-zone silicon for both types of studies.

We do not consider the results given here as positive proof that these bands are to be associated with the divacancy. There is always some degree of uncertainty in such an identification. We do feel, however, that the detailed correlations that have been observed give a strong argument in favor of this identification. One important set of experiments that remains to be done is stress-induced dichroism studies *in situ* at low temperatures. The correlation of the kinetics of the stress induced "electronic" alignment with that observed in the EPR could be conclusive.

Assuming that the identification of these bands with the divacancy is correct, the next step is to identify the nature of the transitions and in turn to learn about the electronic structure of excited states of the defect. In this paper we have made only highly speculative suggestions in this regard based upon the one-electron molecular-orbital model deduced from the EPR studies. Considerable additional experimental work will be required before a detailed assignment can be made. For instance, Rao and Ramdas,[25] in addition to reporting dichroism in the 3.3-μ band noted that for low-temperature measurements the band splits under $\langle 111\rangle$ stress. Such piezospectroscopic effects have been analyzed in detail by Feofilov and Kaplyanskii[31] and will presumably give valuable information concerning the states responsible for the 3.3-μ band. It would be desirable to search at low temperatures with high resolution for the zero-phonon line associated with the 1.8-μ band. If this line can be detected similar piezospectroscopic studies on it become possible.

Finally we note that Kurskii[32] had argued that the 1.8-μ band could be associated with the oxygen-vacancy complex. We have shown that the 1.8-μ band has the wrong symmetry properties and is related to the divacancy so that his suggestion is not correct.

ACKNOWLEDGMENTS

The authors acknowledge the very helpful assistance of J. F. Becker, M. R. Gaerttner, A. H. Kalma, and J. W. Westhead during the performance of all experiments of all experiments in the research program. The authors also thank Dr. H. H. Richtol of the RPI Chemistry Department for giving permission to use the infrared spectrometer and polarizers. We also thark Dr. H. B. Huntington of the RPI Physics Department for interst in this work. Finally, we thank the RPI Linac personnel for their help in the irradiation experiments run using the Linac.

[31] P. P. Feofilov and A. A. Kaplyanskii, Usp. Fiz. Nauk **76**, 201 (1962) [English transl.: Soviet Phys.—Usp. **5**, 79 (1962)].

[32] Yu. A. Kurskii, Fiz. Tverd. Tela. **6**, 2263 (1964) [English transl.: Soviet Phys.—Solid State **6**, 1795 (1965)].

APPENDIX

Here we present the derivation of the dichroism expected from the divacancy model for the X-Y dipoles. We will briefly describe the steps in the derivation and then present the relevant equations without further elaboration.

There are 12 different divacancy configurations. That is, there are four nonequivalent $\langle 111\rangle$ axes, which specifiy the vacancy-vacancy axis, and each of these has three different electron configurations. We will adopt the labeling scheme used in Ref. 18. This scheme can be understood using Fig. 2 of the text. Consider one of the vacancies to be at the center of the cube (at the site labeled c'). The four neighboring silicon atom sites are labeled a, b, c, and d. The first letter of the labeling scheme indicates the position of the other vacancy site (c for the configuration shown in Fig. 2). The second letter denotes the other neighbor silicon site that lies in the X-Y plane of the defect (b in the figure). The divacancy configuration shown in Fig. 2 is thus labeled cb.

Under the applied stress these various configurations become nonequivalent. We will restrict ourselves to the change in energy due to the stress as determined only by the B_3 (or M) component of the strain-energy tensor. This component singles out the strain along the $\langle 110\rangle$ axis which is perpendicular to the X-Y dipole plane. For Fig. 2 this axis is the $[1\bar{1}0]$ axis. The change in energy under stress for the ij defect is therefore simply $M\epsilon_{kl}$, where ϵ_{kl} is the resolved strain along this perpendicular $\langle 110\rangle$ direction. This direction is given by the line between the other two neighbor sites and we have therefore labeled it kl where $k,l\neq i,j$.

The population of the ij defect configuration will in turn reflect the corresponding Boltzmann factor

$$\mathcal{B}_{kl}=\exp\{-M\epsilon_{kl}/kT\}. \tag{A1}$$

The exact relation between these Boltzmann factors and the populations of the configurations is somewhat different for the two types of experiments: electronic- and atomic-reorientation.

In the electronic-reorientation experiment the stress is applied during the measurement. Since the vacancy-vacancy axis cannot change at the temperature of the experiment, the equilibration between populations can take place only among configurations with a common $\langle 111\rangle$ axis, e.g., n_{ab}, n_{ac}, and n_{ad}, and their sum remains constant (equal to the total population before stress, $3N$). Subject to this restriction, the populations of each configuration will be proportional to its corresponding Boltzmann factor given by Eq. (A1), evaluated at 300°K, the temperature of measurement.

In the atomic-reorientation experiments the room-temperature measurements are made in the unstressed state on the frozen-in populations due to equilibration under stress at $\sim$150°C. In this case all of the electronic configurations for a given divacancy axis will be equally

TABLE III. Dichroic ratios for the various experiments.

Stress	$E_\perp/E_\parallel$	Dichroic ratio
[001]	[110]/[001]	$\dfrac{Wn_{ad}+(2-W)n_{ab}}{2(1-W)n_{ad}+2Wn_{ab}}$
[111]	[$\bar{1}\bar{1}$2]/[111]	$\dfrac{X_+n_{ca}+X_-n_{ac}+(2+W)n_{ab}}{Y_-n_{ca}+Y_+n_{ac}+2(1-W)n_{ab}}$
[$\bar{1}\bar{1}$2]	[1$\bar{1}$0]/[$\bar{1}\bar{1}$2]	$\dfrac{6Wn_{ad}+3X_-(n_{ab}+n_{ac})+3X_+(n_{ca}+n_{ba})}{4(1-W)n_{ad}+X_+(2n_{cb}+n_{ca})+X_-(2n_{bc}+n_{ac})+Z_+n_{ab}+Z_-n_{ba}}$
	[1$\bar{1}$0]/[110]	$\dfrac{Wn_{ad}+X_+n_{ba}+X_-n_{ab}}{Wn_{bc}+X_-n_{ba}+X_+n_{ab}}$
[110]	[001]/[110]	$\dfrac{W(n_{ba}+n_{ab})+(1-W)(n_{bc}+n_{ad})}{Wn_{bc}+X_-n_{ba}+X_+n_{ab}}$

populated during the measurement. The total population of a ⟨111⟩ axis will be proportional to the sum of the Boltzmann factors corresponding to the three electronic configurations for that ⟨111⟩, e.g., $n_{ai}\sim\mathfrak{B}_{bc}+\mathfrak{B}_{cd}+\mathfrak{B}_{bd}$. Here the Boltzmann factors are evaluated at 423°K.

The stress directions are shown in Fig. 2 and have been chosen so that the relevant strains ϵ_{kl} can be taken directly from Ref. 16 where they have been previously evaluated.

The dichroic ratio $\mathfrak{D}$, defined as the ratio of the absorption with the light polarized perpendicular to the stress direction to that with the light polarized parallel to the stress is given by

$$\mathfrak{D}=\frac{\alpha_\perp}{\alpha_\parallel}=\frac{\sum_{ij} n_{ij}(P_{ij})_\perp{}^2}{\sum_{ij} n_{ij}(P_{ij})_\parallel{}^2}. \tag{A2}$$

Here n_{ij} is the relative population of the ij configuration, $(P_{ij})_\perp$ is the component of its transition dipole moment P (see Fig. 2 of the text) in the perpendicular polarization direction, and $(P_{ij})_\parallel$ that in the parallel polarization direction. Equation (A2) was evaluated for each of the stress directions and the results are given in Table III in terms of the independent n_{ij}'s. In these tabulated formulas, we employ the following functions:

$$W=\cos^2\theta,$$
$$X_\pm=\tfrac{1}{2}(\cos\theta\pm\sqrt{2}\sin\theta)^2,$$
$$Z_\pm=\tfrac{1}{2}(3\cos\theta\pm\sqrt{2}\sin\theta)^2.$$

Using the Boltzmann factors defined by Eq. (A1) the derived populations n_{ij} to be used in the formulas of Table III are as follows

1. [001] Stress

(a) Electronic

$$n_{ad}=3N\mathfrak{B}_{bc}/(\mathfrak{B}_{bc}+2\mathfrak{B}_{cd})$$
$$(=n_{da}=n_{bc}=n_{cb})$$
$$n_{ab}=3N\mathfrak{B}_{cd}/(\mathfrak{B}_{bc}+2\mathfrak{B}_{cd})$$
$$(n_{ba}=n_{ac}=n_{ca}=n_{bd}=n_{db}=n_{cd}=n_{dc}.$$

(b) Atomic

All ⟨111⟩'s are equivalent and, in the absence of stress during measurement, all n_{ij} are equal, giving $\mathfrak{D}=1$.

2. [111] Stress

(a) Electronic

$$n_{ca}(=n_{cb}=n_{cd})=N,$$
$$n_{ac}=3N\mathfrak{B}_{bd}/(\mathfrak{B}_{bd}+2\mathfrak{B}_{cd})$$
$$(=n_{bc}=n_{dc}),$$
$$n_{ab}=3N\mathfrak{B}_{cd}/(\mathfrak{B}_{bd}+2\mathfrak{B}_{cd})$$
$$(=n_{ba}=n_{ad}=n_{da}=n_{bd}=n_{db}).$$

(b) Atomic

$$n_{ca}=2N\mathfrak{B}_{bd}/(\mathfrak{B}_{bd}+\mathfrak{B}_{cd})$$
$$(=n_{cb}=n_{cd})$$
$$n_{ab}=\tfrac{2}{3}N(2\mathfrak{B}_{cd}+\mathfrak{B}_{bd})/(\mathfrak{B}_{bd}+\mathfrak{B}_{cd})$$
$$(=n_{ac}=n_{ad}=n_{ba}=n_{bc}=n_{bd}=n_{da}=n_{bd}=n_{dc}).$$

3. [$\bar{1}\bar{1}$2] Stress

The relevant strains for this stress were not worked out in Ref. 18 and are

$$\epsilon_{bc}=-\tfrac{1}{12}(2S_{11}+10S_{12}+S_{44})P,$$
$$\epsilon_{ad}=-\tfrac{1}{12}(2S_{11}+10S_{12}+S_{44})P,$$
$$\epsilon_{ac}=-\tfrac{1}{12}(5S_{11}+7S_{12}-2S_{44})P,$$
$$\epsilon_{ab}=-\tfrac{1}{12}(5S_{11}+7S_{12}+2S_{44})P,$$

(a) Electronic

Omitted because this experiment was not performed.

(b) Atomic

$$n_{ba}=2N(2\mathfrak{B}_{ac}+\mathfrak{B}_{ad})/(2\mathfrak{B}_{ac}+2\mathfrak{B}_{ab}+\mathfrak{B}_{ad}+\mathfrak{B}_{bc})$$
$$(=n_{bc}=n_{bd}),$$
$$n_{ca}=2N(2\mathfrak{B}_{ab}+\mathfrak{B}_{ad})/(2\mathfrak{B}_{ac}+2\mathfrak{B}_{ab}+\mathfrak{B}_{ad}+\mathfrak{B}_{bc})$$
$$(=n_{cb}=n_{cd}),$$
$$n_{ab}=2N(\mathfrak{B}_{bc}+\mathfrak{B}_{ac}+\mathfrak{B}_{ab})/(2\mathfrak{B}_{ac}+2\mathfrak{B}_{ab}+\mathfrak{B}_{ad}+\mathfrak{B}_{bc})$$
$$(=n_{ac}=n_{ad}=n_{da}=n_{db}=n_{dc}),$$

4. [110] Stress

(a) Electronic

$$n_{ad}=3N\mathfrak{B}_{bc}/(\mathfrak{B}_{bc}+2\mathfrak{B}_{cd})$$
$$(=n_{da}),$$
$$n_{ab}=3N\mathfrak{B}_{cd}/(\mathfrak{B}_{bc}+2\mathfrak{B}_{cd})$$
$$(=n_{ac}=n_{db}=n_{dc}),$$
$$n_{bc}=3N\mathfrak{B}_{ad}/(\mathfrak{B}_{ad}+2\mathfrak{B}_{cd})$$
$$(=n_{cb}),$$
$$n_{ba}=3N\mathfrak{B}_{cd}/(\mathfrak{B}_{ad}+2\mathfrak{B}_{cd})$$
$$(=n_{bd}=n_{ca}=n_{cd}).$$

(b) Atomic

$$n_{ab}=2N(2\mathfrak{B}_{cd}+\mathfrak{B}_{bc})/(\mathfrak{B}_{bc}+4\mathfrak{B}_{cd}+\mathfrak{B}_{ad})$$
$$(=n_{ac}=n_{ad}=n_{da}=n_{db}=n_{dc})$$
$$n_{ba}=2N(2\mathfrak{B}_{cd}+\mathfrak{B}_{ad})/(\mathfrak{B}_{bc}+4\mathfrak{B}_{cd}+\mathfrak{B}_{ad})$$
$$(=n_{bc}=n_{bd}=n_{ca}=n_{cb}=n_{cd}).$$

PHYSICAL REVIEW VOLUME 152, NUMBER 2 9 DECEMBER 1966

Relationship between the Macroscopic and Microscopic Theory of Crystal Elasticity. I. Primitive Crystals

P. N. KEATING
Bendix Research Laboratories, Southfield, Michigan
(Received 25 July 1966)

The general relationship between the macroscopic theory of crystal elasticity and a recently introduced microscopic formalism is established for primitive crystals. The relationship is more simple and direct than the corresponding relationship between the macroscopic theory and the Born-Huang formalism, which has to be established via sound-wave propagation. Additional conditions are derived for the Born-Huang formalism which remove an inconsistency in the microscopic theory and confirm that purely nearest-neighbor interactions must be central. The new macroscopic-microscopic relationship is applied to an illustrative study of the simple cubic structure which also shows that three of the six third-order elastic constants of the alkali halides depend on long-range interactions.

I. INTRODUCTION

THE Born-Huang coupling-parameter formulation[1] of microscopic elasticity has been in use for some time, and its relationship with the macroscopic formalism has been examined in several articles.[1,2] Recently, a new formalism[3] has been set up for microscopic elasticity which allowed the formal demonstration that a purely nearest-neighbor interaction must be a central one.[3] The new approach offers a number of operational advantages over the Born-Huang formalism which have been demonstrated in calculations of the second-[3] and third-order[4] elasticity of crystals of the diamond type. Thus it has now become advisable to establish the general relationship between this new microscopic approach and the macroscopic formalism so that it can be used more generally. The general relationship is set up for the case of primitive crystals in the present article; the case of nonprimitive crystals exhibits special problems and will be considered in a separate article. We shall show here that, in addition to the advantages mentioned in previous articles,[3,4] the new formulation of macroscopic elasticity allows a more simple and direct formal relationship between macroscopic and microscopic elasticity for primitive crystals than is possible with the Born-Huang approach.

There has also arisen a second problem in the study of the microscopic theory of elasticity. In Ref. 3, hereafter referred to as K, purely first-neighbor interactions were shown to be central. Because the two approaches begin on common ground and are designed to allow the same invariance requirements to be imposed, they should be basically equivalent. However, for certain crystal structures of high symmetry, the Born-Huang

[1] M. Born, K. Huang, *Dynamical Theory of Crystal Lattices* (Oxford University Press, New York, 1954), Chap. V.

[2] See, for example, M. Lax, in *Lattice Dynamics*, edited by R. F. Wallis (Pergamon Press, Inc., New York, 1965), p. 583; G. Leibfried and W. Ludwig, Z. Physik **160**, 80 (1960); R. Srinivasan, Phys. Rev. **144**, 620 (1966).

[3] P. N. Keating, Phys. Rev. **145**, 637 (1966).

[4] P. N. Keating, Phys. Rev. **149**, 674 (1966).